Supplementary Material

Simultaneous enhanced ammonia and nitrate removal from secondary effluent in constructed wetlands using a new manganese-containing substrate

Zhihao Xian [a,b], Jun Yan [a,b], Jingyi Dai [a,b], Hao Wu [a,b], Xin Zhang [a,b], Wenbo Nie [a,b], Fucheng Guo [a,b], Yi Chen [a,b,*]

[a] *Key Laboratory of the Three Gorges Reservoir Region's Eco-Environment, Ministry of Education, Chongqing University, Chongqing 400044, China*

[b] *College of Environment and Ecology, Chongqing University, Chongqing 400044, China*

* Corresponding author. Present address: 174 Shazhengjie Street, Shapingba District, Chongqing 400044, China; Tel.: 86-23-65120750; fax: 86-23-65120750; E-mail address: chenyi8574@cqu.edu.cn (Y. Chen).

Text S1. Measurement of N_2O emission

To determine the emission of N_2O, three acrylic gas collecting hoods with a diameter of 20 cm and height of 30 cm were used, and they were individually placed on top of three CWs (Guo et al., 2020). The hoods were sealed to the CWs with silicone adhesive to prevent gas leakage. Measurement was carried out during each phase three times. The test time was from 8 a.m. to 12 a.m., corresponding to the time of sampling, and the gas samples were collected every hour using a syringe. The gas fluxes were determined based on the gas concentration measured by the gas chromatography unit (GC-2010 Plus, SHIMADZU, Japan) and calculated using the Equation. (S1) (Gu et al., 2022).

$$F = \frac{V}{A} \times \frac{dC_t}{dt} \quad \text{(S1)}$$

Where F is the gas flux (mg/m^2/h); V is the chamber volume (m^3); A is the basal area of the gas chamber (m^2); dC_t/dt is the rate of gas concentration change (mg/m^3/h).

Text S2. Calculation of the average percentage of remaining PCL ester groups

Based on the values of normalized absorbances of MPCM ester groups obtained by FTIR before and after the experiment, the average percentage of remaining MPCM ester groups was calculated by Equation. (S2) (Fukushima et al., 2013).

$$\%De(t) = \frac{(\frac{A_{e(t)}}{A_{CH(t)}})}{(\frac{A_{e0}}{A_{CH0}})} \times 100\% \quad \text{(S2)}$$

Where *%De(t)* is the average percentage of remaining MPCM ester groups at degradation time (t); $A_{e(t)}$ is the normalized absorbance of the MPCM ester groups (1720 cm^{-1}) at degradation time (t); $A_{CH(t)}$ is the absorbance of $–(CH_2)_n–$ stretching groups (731 cm^{-1}) at degradation time (t); A_{e0} is the absorbance of the MPCM ester groups previous to the experiment; A_{CH0} is the absorbance of $–(CH_2)_n–$ stretching groups previous to the experiment.

Text S3. Isotopic tracer incubations

The entire procedure was conducted inside a glovebox filled with high purity helium (He). Before the incubation, substrate slurries were prepared by adding 20 mL sterile anoxic deionized water (with trace element and EDTA-Na at the same concentration as the influent) to approximately 5 mL substrates from sampling sites of three CWs in 100 mL serum vials. Serum vials were sealed with butyl rubber septa and aluminum caps after homogenization. Then, the serum vials were preincubated anoxically in the dark at 24 °C for 24 h to eliminate indigenous oxygen (O_2), nitrite (NO_2^--N) and nitrate (NO_3^--N) while retaining the indigenous reducible MnO_2 almost unchanged. Three treatment groups (n = 3 per treatment group) were established: (1) sterile anoxic deionized water without $^{15}NH_4Cl$ (group-Control), (2) $^{15}NH_4Cl$ addition (^{15}N at 99%, group-$^{15}NH_4Cl$), and (3) $^{15}NH_4Cl$ and acetylene (C_2H_2) addition (group-$^{15}NH_4Cl$ + C_2H_2). As for group-$^{15}NH_4Cl$ and group-$^{15}NH_4Cl$ + C_2H_2, the ultrahigh purity He-purged stock concentrated $^{15}NH_4^+$-N ($^{15}NH_4Cl$) solution was added to reach the concentration of 7 mg/L $^{15}NH_4^+$-N (based on the actual situation in the experiment). For group-$^{15}NH_4Cl$ + C_2H_2, the gas occupying 30% (v/v) of the headspace was evacuated and replaced with C_2H_2. All vials were shaken vigorously to homogenize the slurries and dissolve the C_2H_2.

After 48 h of incubation in the dark at 24 °C, 20 mL of gas samples were collected with gastight syringes and injected into 50 mL air pockets. Isotope ratio mass spectrometry (IRMS, Sercon 20-22) was used to determine the $^{30}N_2$ and $^{29}N_2$ enrichment in the gas samples. The concentrations of $^{30}N_2$ and $^{29}N_2$ were calculated through background subtraction (Zhu et al.,

2013), and the potential Mnammox rates were quantified through the difference in $^{30}N_2$ production with and without $^{15}NH_4Cl$. Additionally, the incubated slurries were sampled immediately after each gas sample was collected to measure the MnO_2 reduction rates based on the production rates of Mn^{2+} concentration during the incubations.

Text S4. Structural equation model

The structural equation model was used to investigate the impact of MPCM and HRT on NH_4^+-N and TN concentrations of the effluent and N_2O emission. Model fit was assessed through several tests such as χ^2 test ($0 < \chi^2/df < 2$, $0.05 < P < 1.00$), high goodness-of-fit index (GFI, $0.9 < GFI < 1.0$), the comparative fit index (CFI, $0.9 < CFI < 1.0$), and the low root means square errors of approximation (RMSEA, < 0.05).

Results showed that the model fit in this experiment was adequate with χ^2/df of 1.469, *P* value of 0.184, GFI of 0.977, CFI of 0.996, and RMSEA of 0.056. The standardized effect value and pathways of the structural equation model were obtained once the model was constructed.

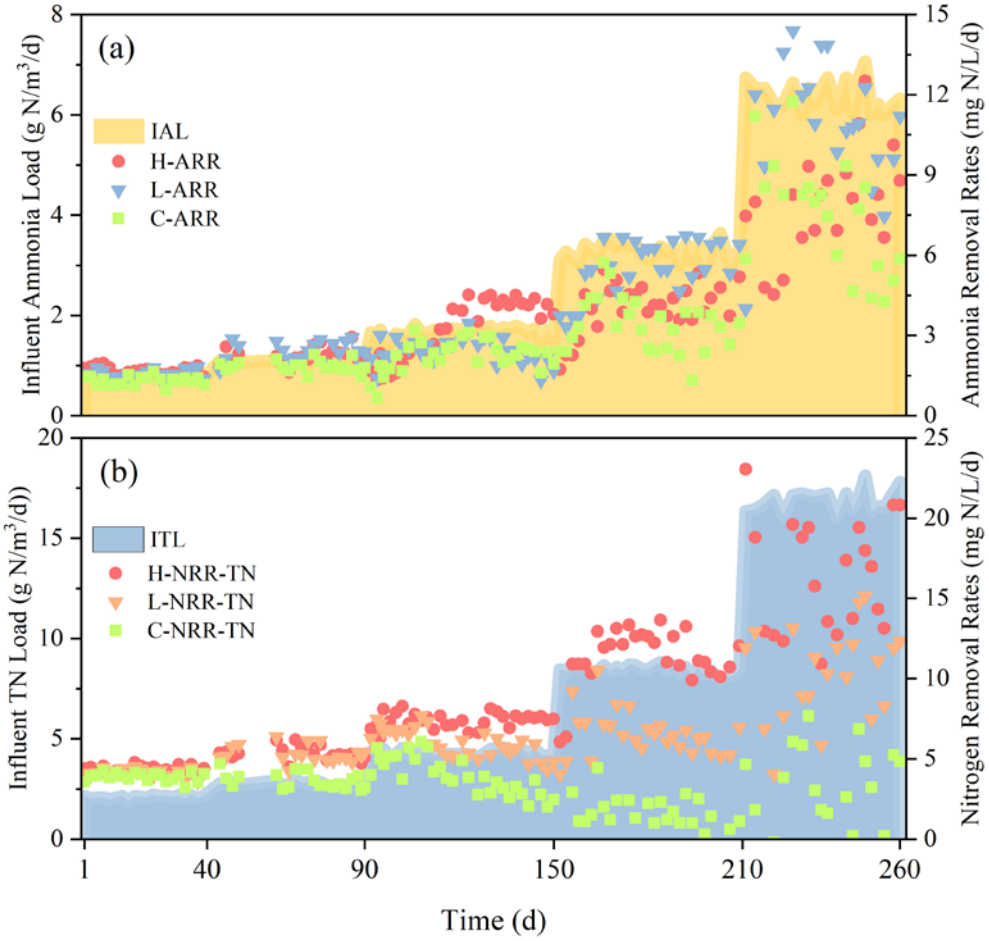

Fig. S1. NH_4^+-N loading rate of influent and NH_4^+-N removal rates during the experiment (a). The nitrogen loading rate of influent and nitrogen removal rates during the experiment (b). H, L, and C are corresponding CWs.

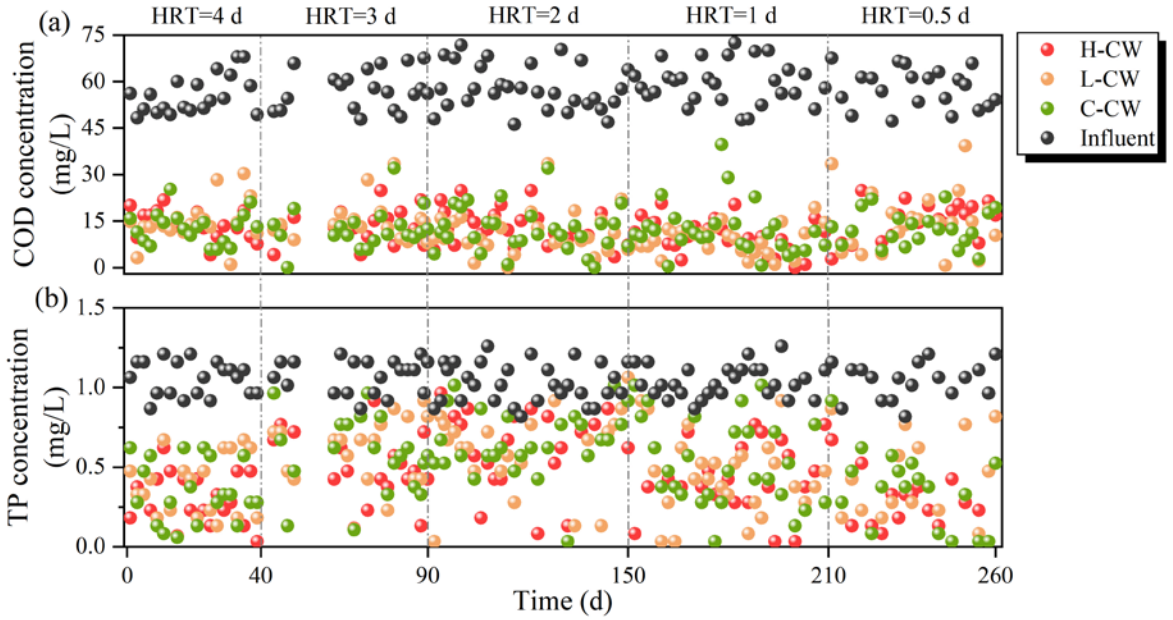

Fig. S2. COD of influent and effluents from the three CWs during the experiment (a). TP of influent and effluents from the three CWs during the experiment (b).

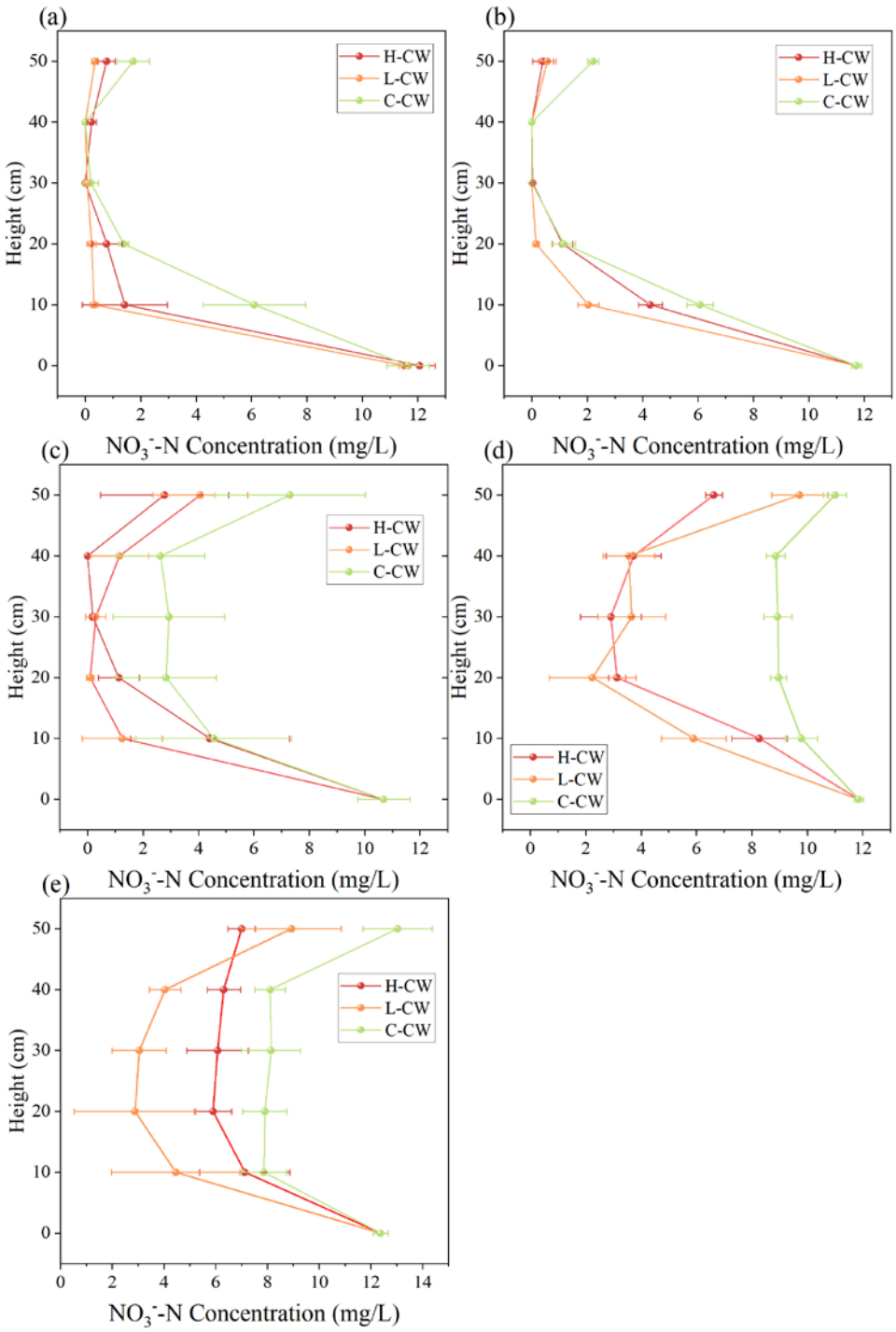

Fig. S3. NO_3^--N concentrations along with the heights of the three CWs in phase 1 (HRT = 4 d, a), phase 2 (HRT = 3 d, b), phase 3 (HRT = 2 d, c), phase 4 (HRT = 1 d, d), and phase 5 (HRT = 0.5 d, e).

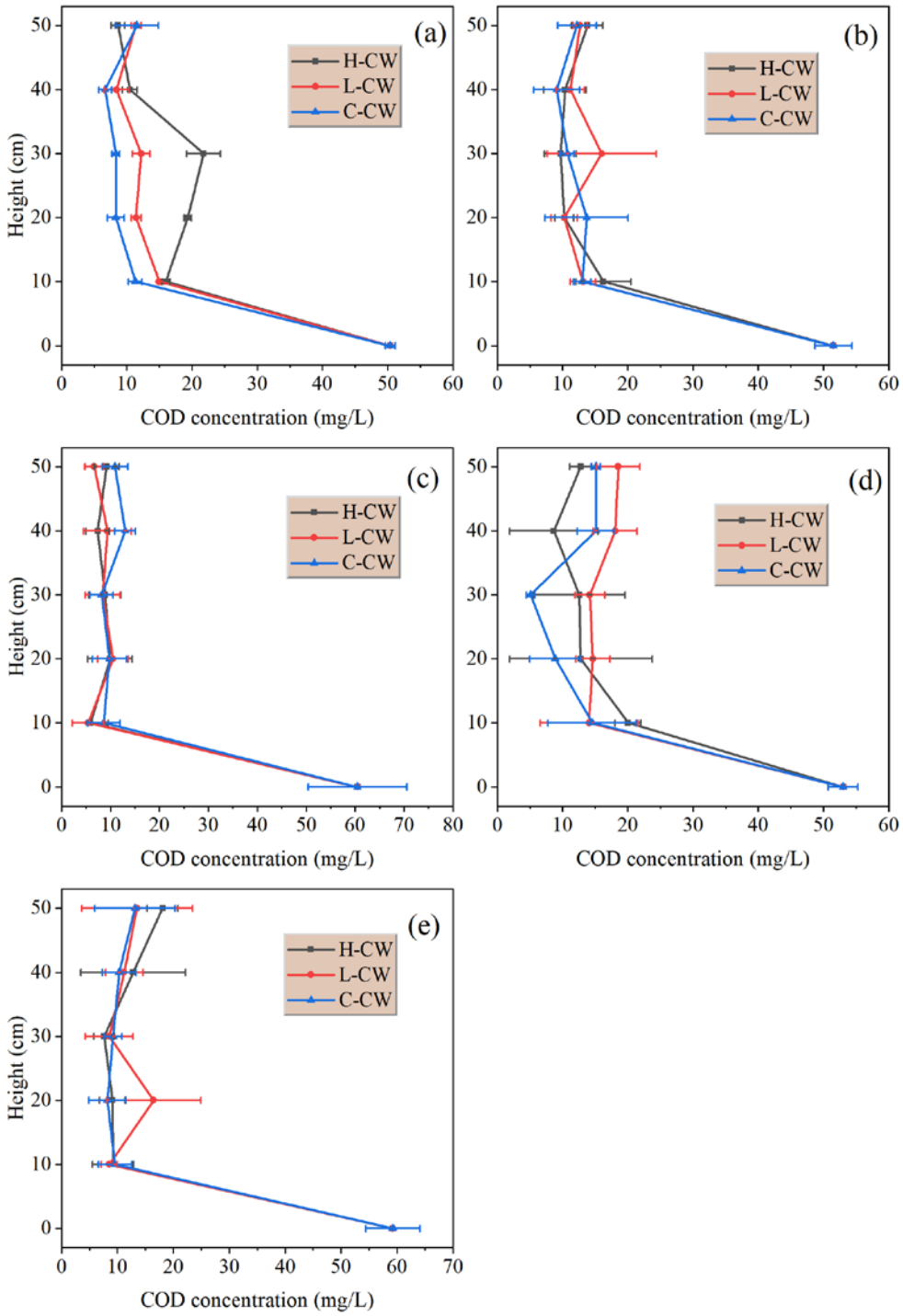

Fig. S4. COD concentrations along with the heights of the three CWs in phase 1 (HRT = 4 d, a), phase 2 (HRT = 3 d, b), phase 3 (HRT = 2 d, c), phase 4 (HRT = 1 d, d), and phase 5 (HRT = 0.5 d, e).

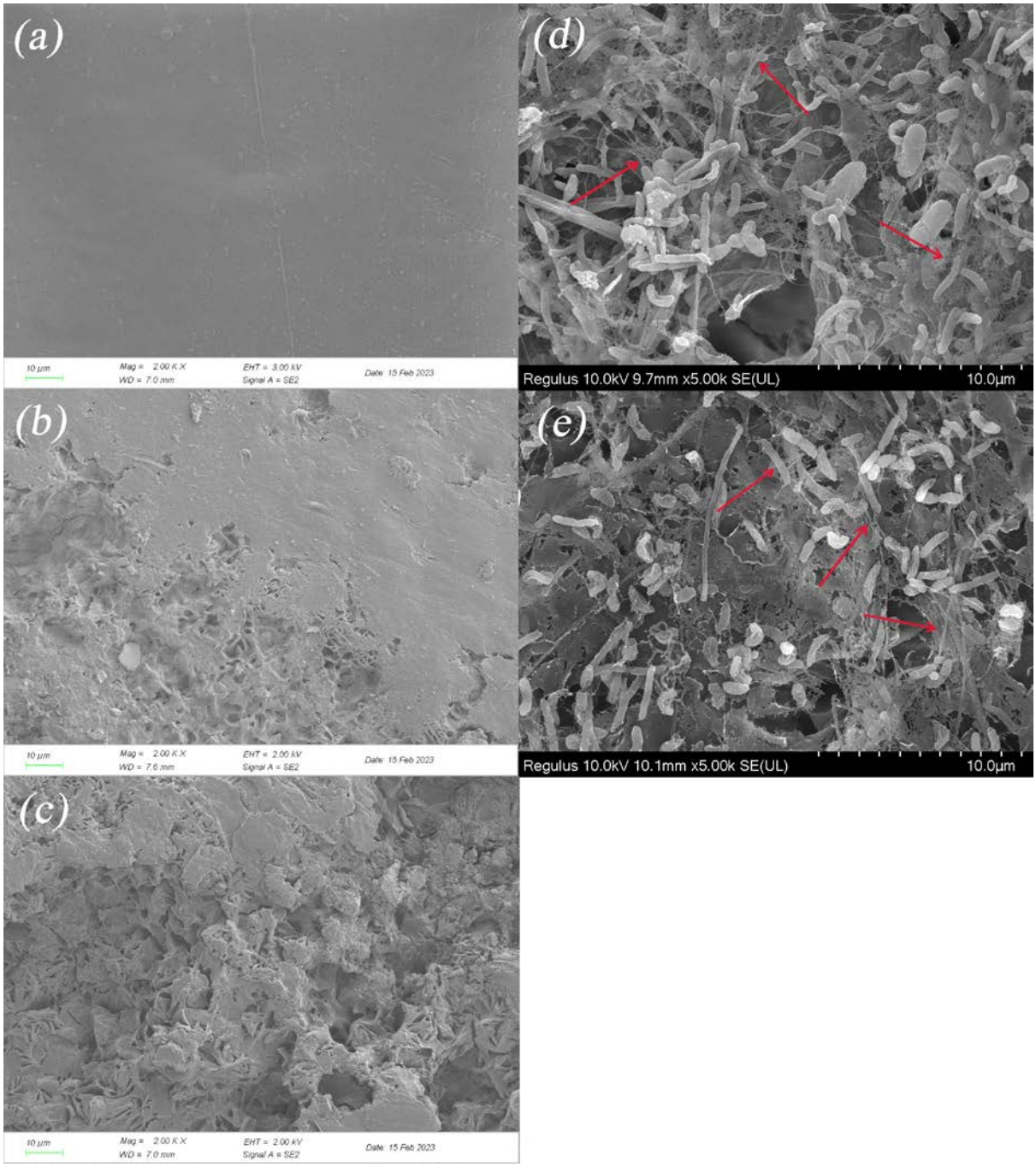

Fig. S5. SEM images of: MPCMs before the experiment (a), MPCM in H-CW after the experiment (b), and MPCM in L-CW after the experiment (c). Biological SEM images of: MPCM with biofilm in H-CW after experiment (d), and MPCM with biofilm in L-CW after experiment (e). (Magnification resp. a, b, c: × 2 k; d, e: × 5 k. The linear structures are indicated by red arrows.)

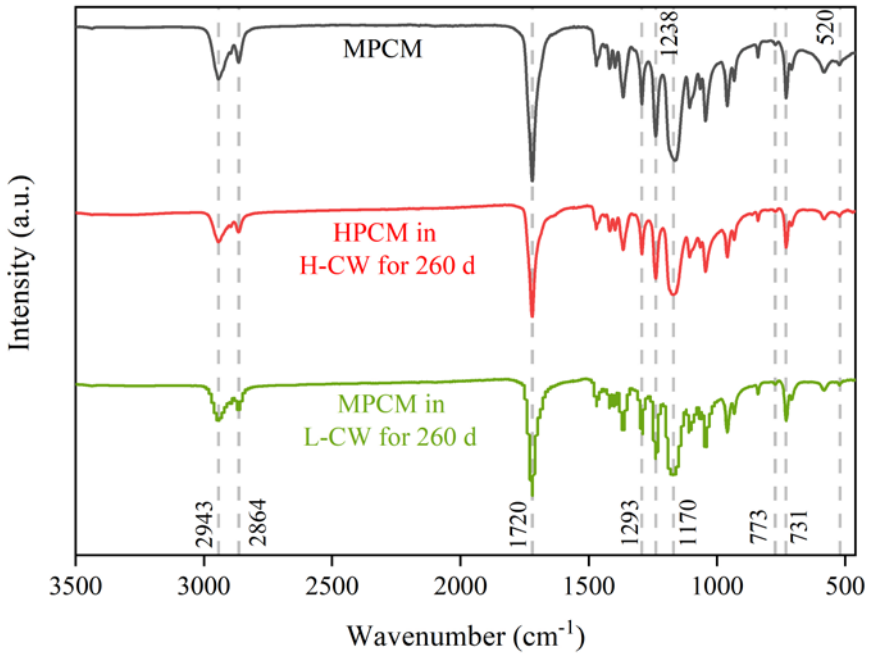

Fig. S6. FTIR spectra of MPCM before and after the experiment. The peak at 731 cm^{-1} belongs to the $–(CH_2)_n–$ stretching groups. The peaks at 1238 and 1170 cm^{-1} are associated with asymmetric and symmetric stretching of *C-O-C*, respectively. The peak at 1293 cm^{-1} is related to *C-O* and *C-C* stretching. The sharp peak at 1720 cm^{-1} belongs to ester groups (*COOR*). The peaks at 2943 and 2864 cm^{-1} corresponded to asymmetric and symmetric stretching of $-CH_2$, respectively. Those mentioned above are similar to previous studies (Kweon et al., 2004; Fukushima et al., 2013; Pereira Barros et al., 2020; Gautam et al., 2021).

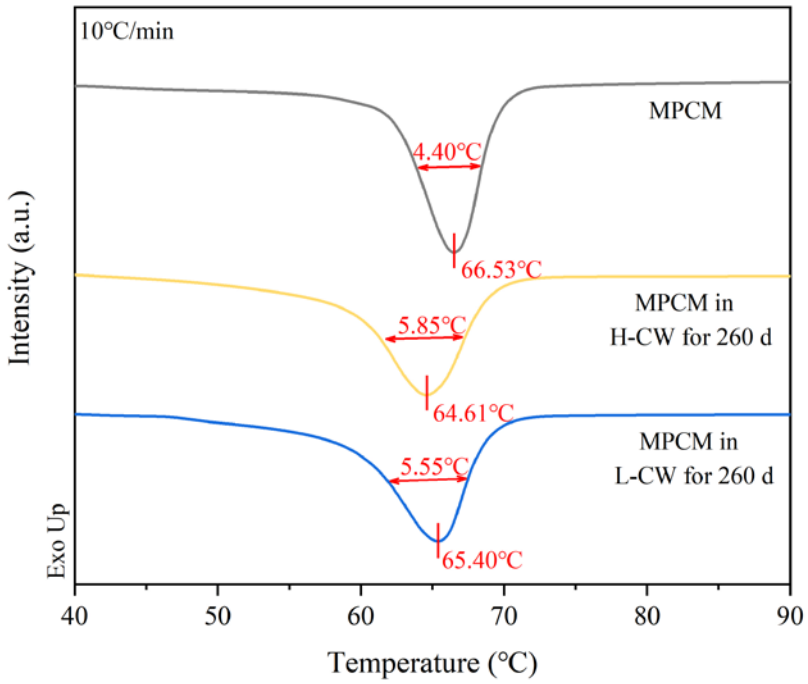

Fig. S7. DSC thermograms of MPCM before and after the experiment. The vertical line indicates the melting temperature. The horizontal line indicates the melting range.

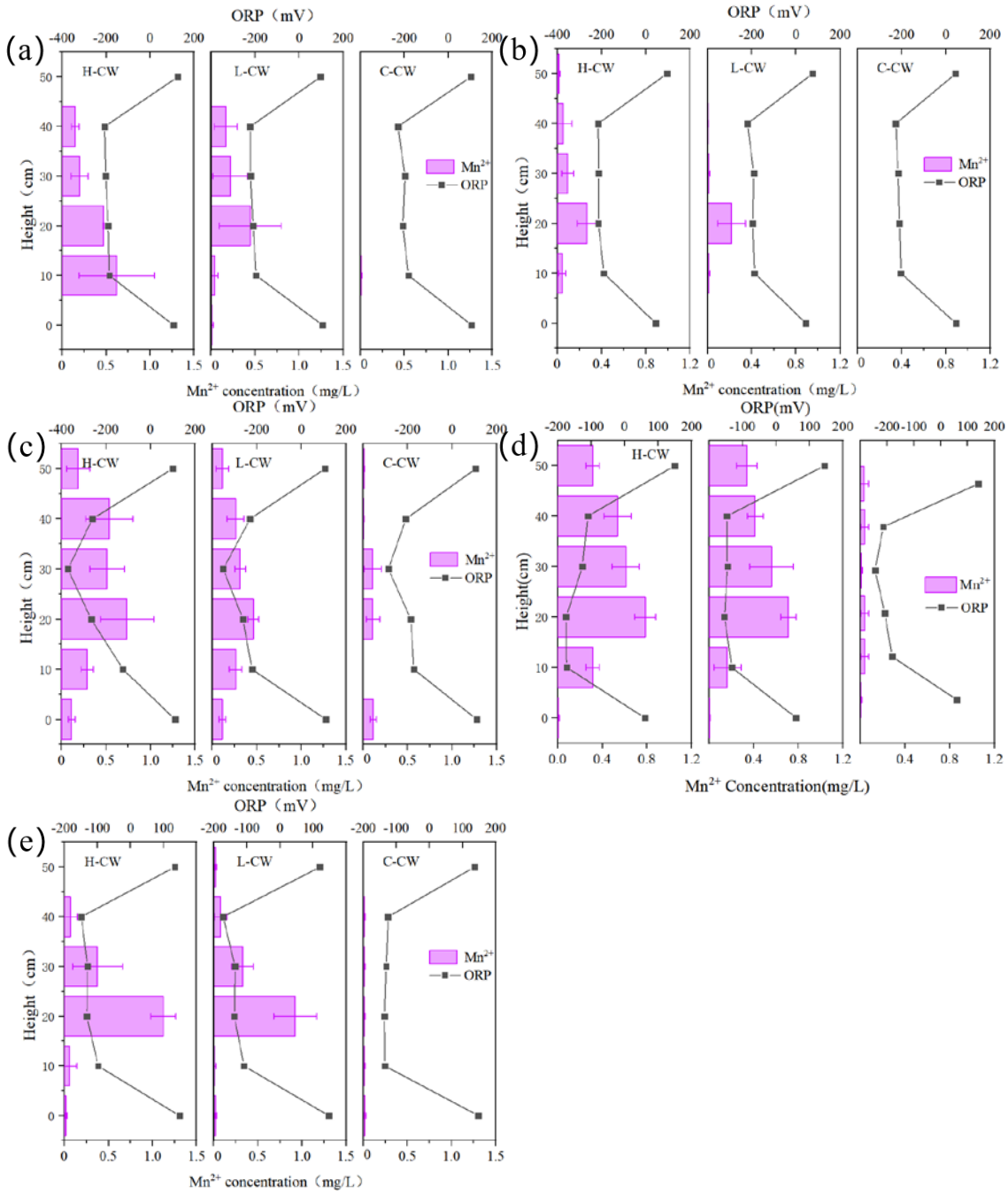

Fig. S8. Mn^{2+} concentrations and ORP values along with the heights of the three CWs in phase 1 (HRT = 4 d, a), phase 2 (HRT = 3 d, b), phase 3 (HRT = 2 d, c), phase 4 (HRT = 1 d, d), and phase 5 (HRT = 0.5 d, e).

Table S1. Comparison of economic costs and nitrogen removal rates with existing CW substrates.

Type of substrates	Influent NH_4^+-N (mg/L)	Influent NO_3^--N (mg/L)	Influent organic matters	NH_4^+-N removal rate (mg N/L/d)	NO_3^--N removal rate (mg N/L/d)	TN removal rate (mg N/L/d)	N_2O emission fluxes ($\mu g/m^2/h$)	Price (RMB/m^3 CW)	Remarks	Types of CWs	Reference
MPCM (H-CW)	8	12	Cellulose (COD=60 mg/L)	8.56	13.11	16.44	40.50	1407.5	Heating at 70°C	Vertical Subsurface Flow (VSF)	H-CW in this study
MPCM (L-CW)	8	12	Cellulose (60)	11.12	6.18	10.34	63.33	703.8	Heating at 70°C	VSF	L-CW in this study
Birnessite sand	8	12	Sucrose (53.5)	2.70	4.00	6.53	-	4229.9	Heating to boiling	VSF	(Cheng et al., 2022a)
Birnessite-coated sand	20	20	Sucrose (50)	6.13	6.03	-	-	4229.9	Heating to boiling	VSF	(Xie et al., 2018)
Birnessite-coated quartz sand	8	-	Glucose (56.3)	-	2.03	-	148	4759.8	Heating to boiling and freeze-drying	VSF	(Cheng et al., 2022b)
Manganese ore	26.03	13.66	Sodium acetate (101)	5.39	4.14	9.38	3100	1481.9	-	VSF	(Cheng et al., 2021)
Iron ore	26.03	13.66	Sodium acetate (101)	2.98	4.35	8.97	4390	279.1	-	VSF	(Cheng et al., 2021)
Manganese ore	13.84	-	Not mentioned	9.19	-	-	-	4094.4	Aeration in CW*	VSF	(Li et al., 2021a)
Pyrite	-	35	Sodium acetate (150)	-	21.8	-	-	2080.2	-	VSF	(Si et al., 2021)
Modified *canna* leaves supported on nZVI	-	50	(200)	-	48.0	-	-	3046.9 (The lifespan is nine days)	Drying at 60°C and heating at 100°C	VSF	(Zhao et al., 2019)
Modified rice straw supported	-	50	(200)	-	46.0	-	-	3038.6 (The lifespan	Drying at 60°C and	VSF	(Zhao et al., 2019)

on nZVI								is nine days)	heating at 100°C		
Modified peanut shell supported on nZVI	-	50	(200)	-	47.0	-	-	3014.8 (The lifespan is nine days)	Drying at 60°C and heating at 100°C	VSF	(Zhao et al., 2019)
Typha latifolia biochar	-	20	Cellulose + Starch (60)	-	4.39	3.99	-	226.3	Pyrolyzing at 300°C	VSF	(Guo et al., 2023)
Eucalypt wood mulch	33	0.2	Glucose (63)	46.83	-8.73	38.25	-	1212.1	195% COD increased in the effluent	VSF	(Saeed and Sun, 2011)
Cornstarch/PCL blends (11:6)	-	50	-	-4.88	41.93	-	-	342.0	Extrusion blending and significant increase of TOC in effluent	Vertical Flow (VF, liquid surface over substrate)	(Shen et al., 2015)
Typha latifolia biochar	8	12	Cellulose + Starch (60)	2.56	3.39	5.38	41.99	181.0	Pyrolyzing at 600°C	VSF	(Zheng et al., 2022)
PCL	6.71	7	-	13.42	8.74	21.44	-	865.0	Aeration in CW*	VSF	(Wang et al., 2023)
PHBV/PLA blends (1:1)	5	10	-	6.68	19.52	19.08	-	1089.1	Significant increase of COD in effluent	VF	(Yang et al., 2018)
PHBV/PLA blends (1:1)	5	10	-	9.18	18.64	27.30	-	1089.1	Aeration in CW* and significant increase of COD in effluent	VF	(Yang et al., 2018)
PHBV/PLA blends (1:1)	3.56	0.162	(33.8)	1.45	0.05	2.18	-	162.9	Heating at 190°C and	Horizontal subsurface	(Jia et al., 2021)

									Aeration in CW*	flow (HSF)	
Hydrophilic cotton microfiber + PBS	25	14	Sucrose (100)	16.28	-	24.65	-	727.43	-	Hybrid VSF (unsaturated zone + saturated zone)	(Zheng et al., 2021)
PBS	25	14	Sucrose (100)	14.67	-	23.50	-	638.74	-	Hybrid VSF (unsaturated zone + saturated zone)	(Zheng et al., 2021)

Note: The removal rate referred to in the table refers to the mean removal rate during the period with the best removal effect. The N_2O emission fluxes referred to in the table refers to the mean emission fluxes. The price mentioned in the table refers to the price of the substrates in the group with the maximum nitrogen removal rate. When the literature does not explicitly mention a price, the price will be estimated based on the 2023 price year from the http://www.alibaba.com/, https://www.aladdin-e.com/zh_cn/ and https://www.taobao.com/. The price only includes the material cost of the substrates and does not include the energy losses involved in the manufacturing, as detailed in the *Remarks* column (* indicates the process during the operation of CWs). For biochar in the table, if the raw material is collected in the field, there may be no cost involved.

Specifically, the link of quartz sand is https://www.alibaba.com/product-detail/Silica-Quartz-Sand_60373262217.html?spm=a2700.galleryofferlist.normal_offer.d_image.72d618abfg5D9j;

the link of manganese ore is https://www.alibaba.com/product-detail/cheapest-price-Manganese-Ore_1700001729695.html?spm=a2700.galleryofferlist.normal_offer.d_image.6f657ae3B1R8nj;

the link of iron ore is https://www.alibaba.com/product-detail/Iron-ore-bulk-quantity-big-size_1600193908661.html?spm=a2700.galleryofferlist.normal_offer.d_image.1f8242fcpWaORw;

the link of pyrite is https://www.alibaba.com/product-detail/High-quality-and-latest-design-ferrous_11000006514303.html?spm=a2700.galleryofferlist.normal_offer.d_image.370a3981LMLO3n;

the link of volcanic rock is https://www.alibaba.com/product-detail/lava-stone-wall-veneer-Red-Lava_1600743313678.html?spm=a2700.galleryofferlist.p_offer.d_image.64c73615fDkyxZ&s=p;

the link of online store selling plant tissues is https://m.1688.com/winport/b2b-2209672599863a35b7.html?share_token=MbmTPaafc2TwKr4OS6nrmDDgVs2s19Dgdt1JnBh76YUDKYcz4f8O/g==&__share_id=dfa4eaff-7e02-4f32-aadc-3b617a037c23&_tabId_=offerlist&spm=a262eq.8992535/20230930.5103953.0&__removesafearea__=1&cbu_sv_id=d3fa2b75-8249-41eb-a29d-08e67ee3cfe9&src_cna=zhCfHetinl8CAXdWsSGbcjFz&visitorId=d3fa2b75-8249-41eb-a29d-08e67ee3cfe9&isVisited=true;

the link of *Typha latifolia* is https://www.alibaba.com/product-detail/Dried-Natural-Jumbo-latifolia-typha-angustifolia_62295609930.html?spm=a2700.galleryofferlist.normal_offer.5.51771e

b5OdbkRk;

the link of eucalypt wood mulch is https://www.alibaba.com/product-detail/Factory-Directly-Wholesale-Pine-Orchid-Bark_1600370362837.html?spm=a2700.galleryofferlist.normal_offer.d_title.54f45333jE9HOn;

the link of polymers is https://www.alibaba.com/product-detail/Polycaprolactone-Raw-Material-PCL-Resin-Polycaprolactone_1600442318264.html?spm=a2700.galleryofferlist.p_offer.d_image.53013ad7RsOluh&s=p;

the link of cornstarch is https://www.alibaba.com/product-detail/Low-Moisture-Modified-Cornstarch_11000008912075.html?spm=a2700.galleryofferlist.normal_offer.d_image.3b5aa4efV4hb7L;

the link of plasticizer and coupling agent is https://www.alibaba.com/product-detail/Leading-Manufacturer-of-IOTA-Silicone-oil_60390595285.html?spm=a2700.galleryofferlist.normal_offer.d_image.23914096HcwtWx;

the link of ceramic particle is https://www.alibaba.com/product-detail/Colored-ceramic-particles-china-manufacture-best_1600824807643.html?spm=a2700.galleryofferlist.normal_offer.d_title.12835055iSUhyk.

Table S2. Synthetic influent

Parameter	Concentration (mg/L)
Carbon source	Cellulose (50.64)
Nitrogen source	$NaNO_3$ (72.85), NH_4Cl (30.57)
Other composition	KH_2PO_4 (4.4), $CaCl_2·2H_2O$ (100), $MgCl_2·6H_2O$ (60), $FeCl_2·4H_2O$ (10), EDTA-Na (20), $ZnSO_4·7H_2O$ (0.4), $MnCl_2·4H_2O$ (0.5), $CoCl_2·6H_2O$ (0.6), $CuCl_2·6H_2O$ (0.05), H_3BO_4 (1.0), $NiCl_2·6H_2O$ (0.04), $Na_2MO_4·2H_2O$ (0.06), $NaHCO_3$ (100)

Table S3. Different phases in the whole experiment

Phase	1	2	3	4	5
HRT (d)	4	3	2	1	0.5
Duration (d)	40	50	60	60	50

Table S4. Primers for 16S rRNA gene used in this study and the corresponding qPCR thermal conditions.

Functional gene	Annealing temperature and time	Elongation temperature and time	Primer	Primer sequence
16S rRNA (Liu et al., 2016)	53℃, 30 s	72℃, 45 s	515FmodF	GTGYCAGCMGCCGCGGTAA
			806RmodR	GGACTACNVGGGTWTCTAAT

Table S5. Changes of DO concentrations along the heights of the three CWs in each phase (mg/L)

	Height (cm)	0	10	20	30	40	50
	H-CW	5.47	0.02	0.03	0.02	0.78	6.02
Phase 1	L-CW	5.47	1.05	0.09	0.01	0.86	3.83
	C-CW	5.47	0.51	0.05	0.01	0.98	4.06
	H-CW	5.30	0.32	0.04	0.03	0.43	7.97
Phase 2	L-CW	5.30	0.52	0.18	0.04	0.15	8.24
	C-CW	5.30	0.58	0.32	0.35	1.02	7.96
	H-CW	5.48	0.64	0.22	0.21	0.37	8.29
Phase 3	L-CW	5.48	0.97	0.15	0.13	0.82	7.15
	C-CW	5.48	1.28	0.88	0.75	0.53	6.64
	H-CW	5.96	0.76	0.48	0.03	0.48	5.35
Phase 4	L-CW	5.96	1.15	0.55	0.26	0.76	6.51
	C-CW	5.96	1.79	0.34	0.19	0.16	4.65
	H-CW	6.72	1.18	0.64	0.61	0.78	7.39
Phase 5	L-CW	6.72	0.86	0.72	0.55	0.9	7.85
	C-CW	6.72	1.13	0.84	0.86	0.57	7.17

Table S6. The specific microbial composition in Figs. 6a – c.

Group	Genus	Function	Reference
Fe-related bacteria	*Dechloromonas*	Fe-oxidation	(Wang et al., 2022)
	Rhodoplanes		
	Desulfomicrobium	Feammox	(Desireddy and Chacko, 2021)
	Desulfosporosinus		
Other DMR-related bacteria	*Methylophilus*	Dissimilatory metal reduction	(Liu et al., 2020)
	Anaeromyxobacter		
	Deferrisoma		
	Desulfuromonas		(Wang et al., 2022)
Other Mn-oxidation bacteria	*Zoogloea*	Mn-oxidation	(Cheng et al., 2022b)
	Acinetobacter		
	Rhodobacter		(Brauer et al., 2011)
	Pseudoxanthomonas		(Ashassi-Sorkhabi et al., 2012)
	Microbacterium		(Yang et al., 2013)
	Agromyces		
	Sphingobium		(Yli-Hemminki et al., 2014)
	Halomonas		(Lee et al., 2021)
	Stenotrophomonas		(Barboza et al., 2015)
	Nakamurella		(Wang et al., 2021)
Other AOB	*Nitrosospira*	Ammonia oxidation	(Zhang et al., 2021)
	Candidatus_Accumulibacter		(Zeng et al., 2016)
	Bacillus		(Cheng et al., 2022a)
Ammonia-oxidizing archaea	*Nitrosarchaeum*		(Jung et al., 2018)
	Crenarchaeota		(Li et al., 2021b)
Feammox-related bacteria	*Desulfosporosinus*	Feammox	(Desireddy and Chacko, 2021)
	Desulfomicrobium		
Anammox-related bacteria	*Candidatus_Anammoximicrobium*	Anammox	(Chen et al., 2019)
	Candidatus_Jettenia		
	Steroidobacter		(Wang et al., 2022)
	Candidatus_Brocadia		(Guo et al., 2022)
	Anaeromyxobacter		(Liu et al., 2020)
DNRA-related bacteria	*Lacunisphaera*	DNRA	(Wang et al., 2020)
	Sorangium		
	Actinomyces		
	Syntrophus		
Other autotrophic denitrification bacteria	*Nakamurella*	Mn- autotrophic denitrification	(Wang et al., 2021)
	Zoogloea		(Cheng et al., 2022b)
	Thiothrix	Autotrophic denitrification	(Yang et al., 2018)
	Dechloromonas	Fe- autotrophic denitrification	(Gu et al., 2022)
Other heterotrophic denitrification bacteria	*Steroidobacter*	Heterotrophic denitrification	(Wang et al., 2022)
	Halomonas		
	Aeromonas		(Cheng et al., 2022a)
	Paracoccus		
	Trichococcus		

	Staphylococcus *Paenibacillus* *Flavobacterium* *Clostridium_sensu_stricto_3*	(Yang et al., 2018)
	Anaerolineaceae_UCG-001	(Wang et al., 2022)

References

Ashassi-Sorkhabi H, Moradi-Haghighi M, Zarrini G (2012). The effect of Pseudoxanthomonas sp as manganese oxidizing bacterium on the corrosion behavior of carbon steel. Materials Science & Engineering C-Materials for Biological Applications, 32(2): 303-309

Barboza N R, Amorim S S, Santos P A, Reis F D, Cordeiro M M, Guerra-Sa R, Leao V A (2015). Indirect Manganese Removal by Stenotrophomonas sp and Lysinibacillus sp Isolated from Brazilian Mine Water. Biomed Research International, 2015

Brauer S L, Adams C, Kranzler K, Murphy D, Xu M, Zuber P, Simon H M, Baptista A M, Tebo B M (2011). Culturable Rhodobacter and Shewanella species are abundant in estuarine turbidity maxima of the Columbia River. Environmental Microbiology, 13(3): 589-603

Chen D, Gu X, Zhu W, He S, Wu F, Huang J, Zhou W (2019). Denitrification- and anammox-dominant simultaneous nitrification, anammox and denitrification (SNAD) process in subsurface flow constructed wetlands. Bioresource Technology, 271: 298-305

Cheng C, Bai X, Zhang J, He Q (2022a). Intensified interactions of triclosan and diclofenac mitigation and nitrogen removal in manganese oxide constructed wetlands. Chemical Engineering Journal, 433

Cheng C, He Q, Zhang J, Chai H, Yang Y, Pavlostathis S G, Wu H (2022b). New insight into ammonium oxidation processes and mechanisms mediated by manganese oxide in constructed wetlands. Water Research, 215: 118251

Cheng S, Qin C, Xie H, Wang W, Zhang J, Hu Z, Liang S (2021). Comprehensive evaluation of manganese oxides and iron oxides as metal substrate materials for constructed wetlands from the perspective of water quality and greenhouse effect. Ecotoxicology and Environmental Safety, 221: 112451

Desireddy S, Chacko S P (2021). A review on metal oxide (FeOx/MnOx) mediated nitrogen removal processes and its

application in wastewater treatment. Reviews in Environmental Science and Bio-technology, 20: 697–728

Fukushima K, Feijoo J L, Yang M-C (2013). Comparison of abiotic and biotic degradation of PDLLA, PCL and partially miscible PDLLA/PCL blend. European Polymer Journal, 49(3): 706-717

Gautam S, Sharma C, Purohit S D, Singh H, Dinda A K, Potdar P D, Chou C F, Mishra N C (2021). Gelatin-polycaprolactone-nanohydroxyapatite electrospun nanocomposite scaffold for bone tissue engineering. Materials Science & Engineering C, 119: 111588

Gu X, Chen D, Wu F, Tang L, He S, Zhou W (2022). Function of aquatic plants on nitrogen removal and greenhouse gas emission in enhanced denitrification constructed wetlands: Iris pseudacorus for example. Journal of Cleaner Production, 330

Guo F, Luo Y, Nie W, Xiong Z, Yang X, Yan J, Liu T, Chen M, Chen Y (2023). Biochar boosts nitrate removal in constructed wetlands for secondary effluent treatment: Linking nitrate removal to the metabolic pathway of denitrification and biochar properties. Bioresource Technology, 379: 129000

Guo F, Zhang J, Yang X, He Q, Ao L, Chen Y (2020). Impact of biochar on greenhouse gas emissions from constructed wetlands under various influent chemical oxygen demand to nitrogen ratios. Bioresource Technology, 303: 122908

Guo M L, Jiang Y, Xie J X, Cao Q F, Zhang Q, Mabruk A, Chen C J (2022). Bamboo charcoal addition enhanced the nitrogen removal of anammox granular sludge with COD: Performance, physicochemical characteristics and microbial community. Journal of Environmental Sciences, 115: 55-64

Jia L, Sun H, Zhou Q, Zhao L, Wu W (2021). Pilot-scale two-stage constructed wetlands based on novel solid carbon for rural wastewater treatment in southern China: Enhanced nitrogen removal and mechanism. J Environ Manage, 292: 112750

Jung M Y, Islam M A, Gwak J H, Kim J G, Rhee S K (2018). Nitrosarchaeum koreense gen. nov., sp nov., an aerobic and mesophilic, ammonia-oxidizing archaeon member of the phylum Thaumarchaeota isolated from agricultural soil.

International Journal of Systematic and Evolutionary Microbiology, 68(10): 3084-3095

Kweon D-K, Kawasaki N, Nakayama A, Aiba S (2004). Preparation and characterization of starch/polycaprolactone blend. Journal of Applied Polymer Science, 92(3): 1716-1723

Lee C J, Wright M H, Bentley S R, Greene A C (2021). Draft Genome Sequence of Halomonas sp. Strain KAO, a Halophilic Mn(II)-Oxidizing Bacterium. Microbiology Resource Announcements, 10(8)

Li Y, Bai X, Ding R, Lv W, Long Y, Wei L, Xiang F, Wang R (2021a). Removal of phosphorus and ammonium from municipal wastewater treatment plant effluent by manganese ore in a simulated constructed wetland. Environ Sci Pollut Res Int, 28(30): 41169-41180

Li Y, Liang Y, Zhang H, Liu Y, Zhu J, Xu J, Zhou Z, Ma J, Liu K, Yu F (2021b). Variation, distribution, and diversity of canonical ammonia-oxidizing microorganisms and complete-nitrifying bacteria in highly contaminated ecological restoration regions in the Siding mine area. Ecotoxicology and Environmental Safety, 217: 112274

Liu C, Zhao D, Ma W, Guo Y, Wang A, Wang Q, Lee D J (2016). Denitrifying sulfide removal process on high-salinity wastewaters in the presence of Halomonas sp. Applied Microbiology and Biotechnology

100(3): 1421-1426

Liu W, Xiao H, Ma H, Li Y, Adyel T M, Zhai J (2020). Reduction of methane emissions from manganese-rich constructed wetlands: Role of manganese-dependent anaerobic methane oxidation. Chemical Engineering Journal, 387: 123402

Pereira Barros J J, Dayane Dos Santos Silva I, Jaques N G, Lia Fook M V, Ramos Wellen R M (2020). Influence of PCL on the epoxy workability, insights from thermal and spectroscopic analyses. Polymer Testing, 89

Saeed T, Sun G (2011). Enhanced denitrification and organics removal in hybrid wetland columns: comparative experiments. Bioresource Technology, 102(2): 967-974

Shen Z, Zhou Y, Liu J, Xiao Y, Cao R, Wu F (2015). Enhanced removal of nitrate using starch/PCL blends as solid carbon

source in a constructed wetland. Bioresource Technology, 175: 239-244

Si Z, Song X, Wang Y, Cao X, Wang Y, Zhao Y, Ge X (2021). Natural pyrite improves nitrate removal in constructed wetlands and makes wetland a sink for phosphorus in cold climates. Journal of Cleaner Production, 280

Wang D, Lin H, Ma Q, Bai Y, Qu J (2021). Manganese oxides in Phragmites rhizosphere accelerates ammonia oxidation in constructed wetlands. Water Research, 205: 117688

Wang S, Pi Y, Song Y, Jiang Y, Zhou L, Liu W, Zhu G (2020). Hotspot of dissimilatory nitrate reduction to ammonium (DNRA) process in freshwater sediments of riparian zones. Water Research, 173: 115539

Wang Y, Song X, Cao X, Xu Z, Huang W, Wang Y, Ge X (2022). Integration of manganese ores with activated carbon granules into CW-MFC to trigger anoxic electron transfer and removal of ammonia nitrogen. Journal of Cleaner Production, 334: 130202

Wang Y, Zhou P, Song X, Xu Z (2023). Simultaneous nitrification and denitrification in a PCL-supported constructed wetland with limited aeration. Environ Sci Pollut Res Int, 30(9): 22606-22616

Xie H, Yang Y, Liu J, Kang Y, Zhang J, Hu Z, Liang S (2018). Enhanced triclosan and nutrient removal performance in vertical up-flow constructed wetlands with manganese oxides. Water Research, 143: 457-466

Yang W H, Zhang Z, Zhang Z M, Chen H, Liu J, Ali M, Liu F, Li L (2013). Population Structure of Manganese-Oxidizing Bacteria in Stratified Soils and Properties of Manganese Oxide Aggregates under Manganese-Complex Medium Enrichment. PLoS One, 8(9)

Yang Z, Yang L, Wei C, Wu W, Zhao X, Lu T (2018). Enhanced nitrogen removal using solid carbon source in constructed wetland with limited aeration. Bioresource Technology, 248: 98-103

Yli-Hemminki P, Jorgensen K S, Lehtoranta J (2014). Iron-Manganese Concretions Sustaining Microbial Life in the Baltic Sea: The Structure of the Bacterial Community and Enrichments in Metal-Oxidizing Conditions. Geomicrobiology

Journal, 31(4): 263-275

Zeng W, Li B X, Wang X D, Bai X L, Peng Y Z (2016). Influence of nitrite accumulation on "Candidatus Accumulibacter" population structure and enhanced biological phosphorus removal from municipal wastewater. Chemosphere, 144: 1018-1025

Zhang Q, Yang Y, Chen F, Zhang L, Ruan J, Wu S, Zhu R (2021). Effects of hydraulic loading rate and substrate on ammonium removal in tidal flow constructed wetlands treating black and odorous water bodies. Bioresource Technology, 321: 124468

Zhao Y, Song X, Cao X, Wang Y, Zhao Z, Si Z, Yuan S (2019). Modified solid carbon sources with nitrate adsorption capability combined with nZVI improve the denitrification performance of constructed wetlands. Bioresour Technol, 294: 122189

Zheng F, Fang J, Guo F, Yang X, Liu T, Chen M, Nie M, Chen Y (2022). Biochar based constructed wetland for secondary effluent treatment: Waste resource utilization. Chemical Engineering Journal, 432

Zheng X, Zhang J, Li M, Zhuang L L (2021). Optimization of the pollutant removal in partially unsaturated constructed wetland by adding microfiber and solid carbon source based on oxygen and carbon regulation. Sci Total Environ, 752: 141919

Zhu J, Mulder J, Bakken L, Dorsch P (2013). The importance of denitrification for N2O emissions from an N-saturated forest in SW China: results from in situ N-15 labeling experiments. Biogeochemistry, 116(1-3): 103-117